

Viscous Control of Peeling an Elastic Sheet by Bending and Pulling

John R. Lister and Gunnar G. Peng

*Institute of Theoretical Geophysics, Department of Applied Mathematics and Theoretical Physics,
University of Cambridge, Wilberforce Road, Cambridge CB3 0WA, United Kingdom*

Jerome A. Neufeld

*BP Institute, Department of Earth Sciences, Department of Applied Mathematics and Theoretical Physics,
University of Cambridge, Bullard Laboratories, Madingley Road, Cambridge CB3 0EZ, United Kingdom*
(Received 31 December 2012; published 7 October 2013)

Propagation of a viscous fluid beneath an elastic sheet is controlled by local dynamics at the peeling front, in close analogy with the capillary-driven spreading of drops over a precursor film. Here we identify propagation laws for a generic elastic peeling problem in the distinct limits of peeling by bending and peeling by pulling, and apply our results to the radial spread of a fluid blister over a thin prewetting film. For the case of small deformations relative to the sheet thickness, peeling is driven by bending, leading to radial growth as $t^{7/22}$. Experimental results reproduce both the spreading behavior and the bending wave at the front. For large deformations relative to the sheet thickness, stretching of the blister cap and the consequent tension can drive peeling either by bending or by pulling at the front, both leading to radial growth as $t^{3/8}$. In this regime, detailed predictions give excellent agreement and explanation of previous experimental measurements of spread in the pulling regime in an elastic Hele-Shaw cell.

DOI: [10.1103/PhysRevLett.111.154501](https://doi.org/10.1103/PhysRevLett.111.154501)

PACS numbers: 47.15.gm, 47.20.Ma, 47.55.np

The viscous spreading of fluid beneath an elastic sheet is controlled by dynamics at the peeling front, in close analogy to the control exerted by the contact line in the capillary spreading of drops over a precursor film. Dynamical control of fluid-mediated elastic peeling can be found in, for example, the manufacture of flexible electronics and microelectromechanical systems (MEMS) [1,2], the reopening of airways [3,4], the suppression of viscous fingering in a deformable Hele-Shaw cell [5,6], and the geological formation of laccoliths [7,8] by the lateral flow of lava beneath an elastic sediment layer.

The controlling influence of contact lines in the related problem of surface-tension driven spreading has long played an important role in our physical understanding of the dynamics of wetting [9]. In surface-tension driven problems, on length scales smaller than the capillary length, $L_c = \sqrt{\gamma/\rho g}$, gravity is negligible (for surface energy γ and fluid density ρ). In this limit, an assumption that the thickness of droplet $h = 0$ at the contact line leads to divergent viscous stresses, and hence to the theoretical immobility of contact lines [10]. This apparent paradox, which conflicts with everyday experience of spreading droplets, can be resolved by considering the development of a precursor film due to intermolecular interactions (van der Waals for example) in advance of the contact line [9]. There, a local balance between viscous dissipation and the rate of change of surface energy gives rise to Tanner's law [11,12], in which the droplet radius advances with speed $dR/dt \propto \theta^3$ for apparent contact angle θ , and thus R increases as $t^{1/10}$.

In the elastic case considered here, we show that while propagation is similarly controlled by dynamics at the

peeling front, the dominant balance is now between viscous forces and elastic bending and tension. The result is a rich set of solution behaviors in which spreading is governed by peeling-by-bending or peeling-by-pulling conditions at the peeling front.

We examine the peeling-by-bending regime theoretically and experimentally in the geometry illustrated in Fig. 1. An axisymmetric fluid blister of thickness $h(r, t)$ is formed by a volumetric flux Q of viscous fluid injected below an elastic sheet of thickness d that rests on a thin prewetting layer of fluid of thickness h_0 and viscosity μ . When the vertical deflection of the elastic sheet is small compared to its thickness, $h \ll d$, we can neglect stretching of the sheet and consider only bending stresses. The fluid pressure is the sum of elastic and hydrostatic components; in this case $p = B\nabla^4 h + \rho g(h - z)$, where $B = Ed^3/12(1 - \nu^2)$ is the bending stiffness of the sheet, and E and ν are the Young's modulus and Poisson's ratio. Lateral gradients in this pressure drive flow and thus,

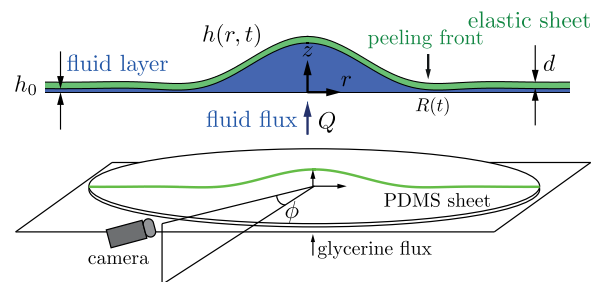


FIG. 1 (color online). Schematic of the model and experimental setup.

within the lubrication approximation, the evolution of the elastic sheet deflection and a global statement of mass conservation are given by [7]

$$\frac{\partial h}{\partial t} = \frac{1}{12\mu} \nabla \cdot [h^3 \nabla (B \nabla^4 h + \rho g h)], \quad (1)$$

$$Qt = 2\pi \int_0^{R(t)} (h - h_0) r dr, \quad (2)$$

where $R(t)$ is the radial extent of the fluid blister. We can immediately identify in (1) a radial “elastogravity” length scale $L_e = (B/\rho g)^{1/4}$ at which bending stresses and gravity contribute equally to flow; L_e is the analogue of the capillary length L_c . Natural height and time scales for (1) and (2) are $L_h = (12Q\mu/\rho g)^{1/4}$ and $\tau = L_h L_e^2/Q$.

As in the capillary case, gravity is negligible near a contact line, and any requirement that $h \rightarrow 0$ as $r \rightarrow R$ implies divergent viscous stresses or an immobile blister ($dR/dt = 0$) [13] (see the Supplemental Material [14]). In the presence of a prewetting layer, propagation must therefore be determined by matching to a solution for peeling by bending at the blister edge.

At early times, when $R \ll L_e$, we can neglect gravity and consider a simpler peeling problem. For small prewetting film thicknesses, $\epsilon \equiv h_0/L_h \ll 1$, spreading is very slow and the interior has uniform pressure $p = B \nabla^4 h$ with $h = h' = O(\epsilon)$ at $r = R$ and $h' = h''' = 0$ at $r = 0$. Thus the interior solution is

$$h(r, t) = \frac{3Qt}{\pi R^2(t)} \left(1 - \frac{r^2}{R^2(t)}\right)^2. \quad (3)$$

If R is to increase, the elastic sheet near the blister edge must be peeled away from the prewetted substrate by bending. A local traveling-wave solution with speed c of the form $h = h_0 f(x - ct)$ must satisfy

$$-c f' = \frac{B h_0^3}{12\mu} [f^3 (f''''')]'. \quad (4)$$

We define a peeling length scale $L_p = (B h_0^3 / 12\mu c)^{1/5}$, and solve $F^3 F^{(v)} + F = 1$, where $F[\xi \equiv (x - ct)/L_p] = f(x - ct)$, subject to $F \rightarrow 1$ as $\xi \rightarrow \infty$ and $F''' = F'''' = 0$ and $F'' \rightarrow A$ as $\xi \rightarrow -\infty$, in order to match to the curvature of the interior, constant-pressure, solution (see the Supplemental Material [14]). Solving this system numerically, we find $A = 1.35$ and hence find the dimensional peeling speed in terms of the curvature κ of the interior solution at the tip,

$$\frac{dR}{dt} = c = \frac{B h_0^{1/2}}{12\mu} \left(\frac{\kappa}{1.35}\right)^{5/2}. \quad (5)$$

This new propagation law for peeling by bending is the elastic analogue of Tanner’s law [12] for surface-tension driven spreading, and can be contrasted with previous solutions for inextensible peeling by pulling [15].

Using the new propagation law (5), and the form of the interior solution in (3), we now find that the radius and height of the blister are given by similarity solutions

$$R(t) = 1.31 \left(\frac{h_0 B^2 Q^5}{\mu^2}\right)^{1/22} t^{7/22}, \quad (6)$$

$$h(0, t) = 0.55 \left(\frac{\mu^2 Q^6}{h_0 B^2}\right)^{2/22} t^{8/22}, \quad (7)$$

respectively.

We experimentally examined the dynamics of this peeling-by-bending solution by injecting a viscous fluid under a deformable elastic sheet and accurately measuring the surface deflections through time. The experiments were performed using a 930 ± 2 mm diameter polydimethylsiloxane (PDMS) sheet (Dow Corning Sylgard 184 silicone elastomer) with thickness $d = 10 \pm 0.5$ mm, Young’s modulus $E = 1.82 \pm 0.09$ MPa [16], Poisson’s ratio $\nu = 0.45$, and therefore bending stiffness $B = 0.188$ Pa m³. The PDMS sheet was placed on a rigid Perspex base with a central 15.9 mm diameter hole through which fluid could be injected.

Surface deflections of the PDMS sheet were measured by digitally imaging a predrawn line on the sheet from a known oblique angle ϕ to the horizontal (see Fig. 1) and at right angles to the line. For each experiment the deflection of the line was measured with respect to a reference image of the undeflected line. Subpixel accuracy was achieved by fitting a Gaussian profile across the line (whose width was ~ 1.5 mm), processing the differences between the deflected and reference images, and thereby resolving vertical deflections of order 10 μ m (see the Supplemental Material [14]).

Experiments were prepared by injecting a known small volume of glycerine under the PDMS sheet, and manually spreading the fluid evenly over the full area of the sheet. This provided an estimate of the average prewetting film thickness h_0 . A local measure of the prewetting film thickness was provided by observing deflection of the sheet by a small weight. During the experiment glycerine was injected under the center of the PDMS sheet with a peristaltic pump (Watson-Marlow 502s) and the mass flux measured with a digital scale (Ohaus Adventure Pro) [17].

The results of these experiments are shown in Figs. 2(b) and 3, with comparisons to numerical solutions of the evolution equation (1) for various prewetting film thicknesses h_0 . The data, scaled using the elastogravity length L_e and time scale τ (see Ref. [17]), confirm that the radial extent is a function of the prewetting film thickness h_0 and thus demonstrate the importance of edge control by peeling. The inset shows the comparison between the experimental profiles for $\epsilon = 0.035$ and 0.054 with the numerical solutions of (1) and (4) for the peeling-by-bending wave. We can see evidence for the flexural wave, with a dimensional amplitude of about 30 μ m.

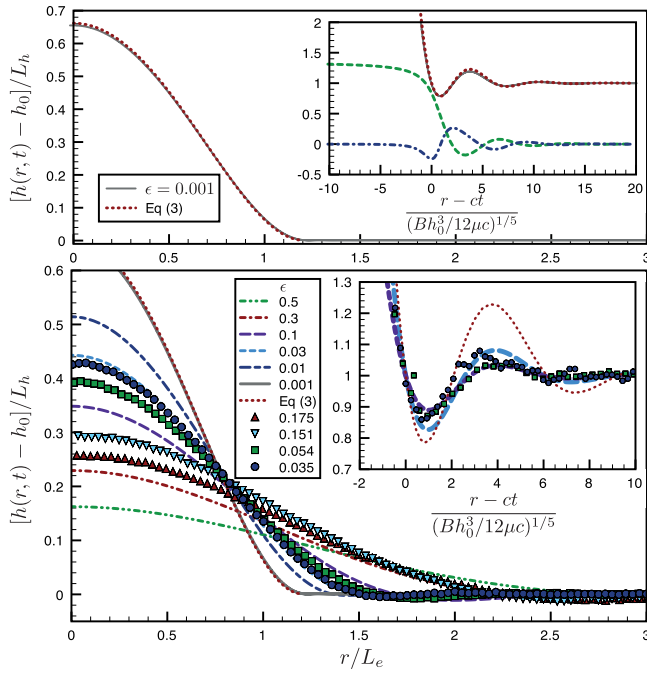


FIG. 2 (color online). Asymptotic, numerical and experimental profiles of the elastic blister at $t/\tau = 1$. (a) Asymptotic and numerical solutions for $\epsilon \equiv h_0/L_h = 0.001$. Inset shows the peeling-by-bending traveling-wave solution F to (4). (b) Experimental profiles for $\epsilon = 0.035, 0.054, 0.151$, and 0.175 , with other experimental parameters detailed in Ref. [17], and numerical solutions for $\epsilon = 0.5, \dots, 0.001$. Inset shows the scaled experimental profiles at the blister edge for $\epsilon = 0.035$ and 0.054 with numerical solutions for $\epsilon = 0.03$ and 0.1 .

Figure 3 shows the radial extent (top) and central height of the blister (bottom) as functions of the scaled time. For $\epsilon \ll 1$ and $R \ll L_e$ there is excellent agreement with the similarity solutions (6) and (7) [18]. For $R \gg L_e$ there is a clear transition to a new regime because gravity can no longer be neglected in the form of the interior solution.

At intermediate times, when $\epsilon \ll 1$ and $R \gg L_e$, peeling by bending continues to control propagation but gravity now plays an increasing role in the interior. The interior blister remains quasistatic with negligible horizontal pressure gradients and satisfies $L_e^4 \nabla^4 h + h = \text{constant}$ with $h(R) = h'(R) = 0$ and $h' = h''' = 0$ at $r = 0$. Solutions have the asymptotic form of an interior flat-topped region, of height h_i , with a peripheral bending region of width $O(L_e)$, where

$$h(y) = h_i [1 - e^{-y}(\cos y + \sin y)] \quad (8)$$

and $y = (R - r)/\sqrt{2}L_e$. This is the elastic analogue of a sessile drop at large Bond number, which forms a flat-topped puddle with a peripheral meniscus on the scale of the capillary length [19].

The interior curvature of (8) at the peeling front, $r = R$, is now $\kappa = h_i/L_e^2$, and the volume constraint (2) gives $h_i \approx Qt/(\pi R^2)$. The elastic spreading law (5) thus implies

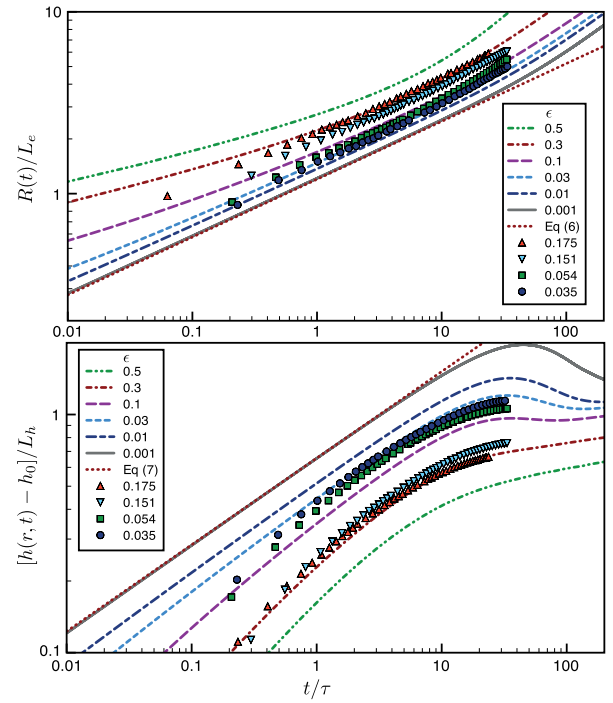


FIG. 3 (color online). Numerical and experimental results, with similarity solutions (6) and (7) for $\epsilon = 0.001$. (a) Dimensionless radius with time. (b) Dimensionless height at the origin with time.

$$R(t) = 0.40 \left(\frac{\rho g}{B} \right)^{5/24} \left(\frac{h_0 B^2 Q^5}{\mu^2} \right)^{1/12} t^{7/12}, \quad (9)$$

$$h(0, t) = 2.02 \left(\frac{B}{\rho g} \right)^{5/12} \left(\frac{\mu^2 Q}{h_0 B^2} \right)^{1/6} t^{-1/6}. \quad (10)$$

Note that the height is predicted to decrease in this regime, explaining the numerical behavior seen in Fig. 3 for $\epsilon \leq 0.03$.

At late times, where $R \gg L_e \epsilon^{-1/2}$, the pressure drop associated with the interior Poiseuille flow from the source towards the peeling front becomes the dominant resistance to propagation. The flow enters a new regime in which the bending stresses in (1) can be neglected almost everywhere, resulting in a standard viscous gravity-current balance [7,20]. The extent

$$R(t) = 0.715 (\rho g Q^3 / 12 \mu)^{1/8} t^{1/2}, \quad (11)$$

and while bending stresses modify the shape of the gravity-current solution near $r = 0$ and $r = R$, they no longer control the dynamics of propagation.

In summary, for $h_0 \ll h \ll d$ the flow passes through three asymptotic dynamical regimes, as confirmed numerically: pressure-driven peeling with $R(t)$ given by (6) for $R \ll L_e$ (or $t/\tau \ll \epsilon^{-1/7}$); gravity-driven peeling given by (9) for $1 \ll R/L_e \ll \epsilon^{-1/2}$ (or $\epsilon^{-1/7} \ll t/\tau \ll \epsilon^{-1}$); and

a viscous gravity current given by (11) for $R \gg L_e \epsilon^{-1/2}$. Our experiments straddle the first two of these regimes.

A different analysis is required when the deflection $h(r, t)$ of the elastic sheet is large compared to its thickness d . At large Q this could happen even if $h_0 \ll d$ through the $t^{8/22}$ growth in (7) before any transition to (10). In the experiments of Ref. [5], d and h_0 were both in the range 0.33–0.97 mm, and the thinness of their latex sheets meant $h(0, t)/d$ reached values of order 10. In these circumstances, the stretching of the sheet can no longer be neglected when calculating the elastic stresses and fluid pressure.

The Föppl–von Kármán plate equations for an axisymmetric pressurized blister [21] can be written as

$$p = B\nabla^4 h - \frac{1}{r} \frac{d}{dr} \left(rT \frac{dh}{dr} \right), \quad (12)$$

$$\frac{1}{r} \frac{d}{dr} \left(r^3 \frac{dT}{dr} \right) = -\frac{Ed}{2} \left(\frac{dh}{dr} \right)^2, \quad (13)$$

where $T(r, t)$ is the radial tension in the sheet induced by stretching. Scaling shows that for $h \ll d$ the tension term in (12) can be neglected, thus recovering (1). Conversely, for $h \gg d$ the bending term in (12) can be neglected in the interior.

Assuming that a slow peeling process controls the rate of spread, we again expect a constant-pressure interior solution for $h \gg d$. After integration of (12) to find $dh/dr = -rp/2T$ in $r < R$, (13) yields

$$\frac{T^2}{r^3} \frac{d}{dr} \left(r^3 \frac{dT}{dr} \right) = -\frac{Edp^2}{8}. \quad (14)$$

In $r > R$ Eq. (13) yields $T \propto r^{-2}$. We solved (14) numerically subject to regularity at $r = 0$ and the matching condition $(r^2 T)' = 0$ at $r = R$. The solution describes the tension and hence shape of the stretched sheet. The volume constraint (2) gives the fluid pressure as $p = 0.324Ed(Qt)^3/R^{10}$, and the sheet approaches $r = R$ with a contact angle $\theta = 1.64Qt/R^3$ and edge tension $T_\theta = 0.099Ed(Qt/R^3)^2$. (The tension at $r = 0$ is $1.71T_\theta$.) This solution is the elastic analogue of the spherical-cap shape [12] of a capillary drop with a small contact angle.

There are two possibilities for the rate of spread of the pressurized elastic blister, depending on the relative sizes of the peeling length scale L_p and a bending boundary-layer length scale $L_b = (B/T_\theta)^{1/2}$ that arises from a balance of the two terms in (12) near $r = R$:

If $h_0 \ll d$ then there is a static bending boundary layer, where

$$h' = \theta(e^{(r-R)/L_b} - 1), \quad (15)$$

within which is nested a peeling-by-bending traveling-wave solution of the form analyzed in the first part of the Letter. Evaluating the curvature κ from (15) and using the propagation law (5), we deduce that

$$R(t) = 0.783 \left(\frac{Edh_0^2}{B} \right)^{5/64} \left(\frac{BQ^5}{\mu h_0^2} \right)^{1/16} t^{3/8}. \quad (16)$$

Alternatively, if $h_0 \geq d$ then a bending boundary layer is unnecessary since the viscous pressure drop of the peeling wave extends over a length scale h_0/θ greater than L_b . Peeling is then by pulling with tension T_θ , locally like an inextensible tape [15]. Matching the interior solution (14) to the Landau-Levich peeling-by-pulling solution [11] yields a propagation law of Cox-Voinov type,

$$\frac{dR}{dt} = \frac{T_\theta \theta^3}{36\mu \ln(1/\delta)}, \quad (17)$$

where δ is the ratio of inner and outer length scales. (The factor 36, rather than 9 in capillary wetting, arises from the no-slip condition at the sheet.) Combining (17) with the numerical solutions for T_θ and θ gives

$$R(t) = 0.807 \left(\frac{EdQ^5}{\mu \ln(1/\delta)} \right)^{1/16} t^{3/8}, \quad (18)$$

where, for simplicity, we take $\delta = h_0/\theta R$. (An alternative theory, with which we disagree (see the Supplemental Material [14]), is given in Ref. [6].)

In Fig. 4 we compare the experimental data of Ref. [5] with the theoretical prediction (18). We note that there is significantly better collapse of the data than in Fig. 2(b) of Ref. [5], where the scaling differed by a factor $(h_0/d)^{1/8}$ [22], and that there is excellent agreement with the theory.

This agreement might initially be thought surprising since spread in Ref. [5] was driven by gas rather than fluid injection. However, if the prewetting fluid accumulates in the peeling wedge, a simple volume balance shows that its radial extent $x \sim (h_0\theta/R)^{1/2} \propto t^{2/8}$ is greater than the scale $h_0/\theta \propto t^{1/8}$ of the peeling region. Thus the gas is irrelevant to the predicted rate of spread (except perhaps by about 3% if we instead take $\delta = h_0/\theta x$).

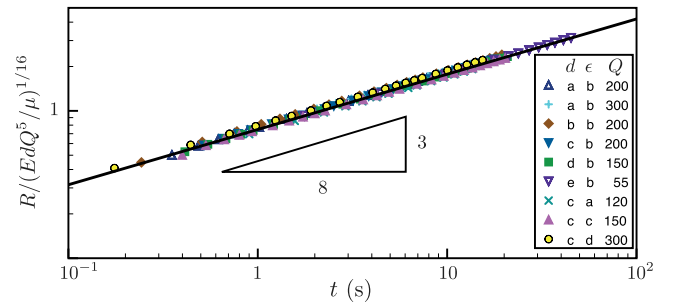


FIG. 4 (color online). Collapse of experimental data from a Hele-Shaw cell with an elastic wall [5]. The raw data are the same as in their Fig. 2(a), and is replotted with approximately corresponding symbols for a range of flow rates Q [$\text{cm}^3 \text{min}^{-1}$], sheet thickness d (their h), and prewetting film thickness h_0 ; h_0/d varies from 0.57 to 1.7. See Ref. [5] for details. An average value $1/\delta \approx 30$ was used when evaluating the line $0.748t^{3/8}$ from (18).

Late-time suppression of Saffman-Taylor fingering in Ref. [5] can be explained by the decrease in the capillary number [23], but not, on its own, the complete suppression of instability for small Q . We hope that our theoretical solution for the radial base state will shed light on the instability mechanism. More importantly, we have shown here that elastic peeling away from a prewetting film is the dominant control on propagation in a suite of problems. Peeling by bending according to (5) is a novel variation on peeling by pulling at the tip (17).

We thank D. Vella for many valuable discussions about these problems. M. A. Hallworth assisted with the experiments. J. A. N. is supported by a Royal Society University Research Fellowship.

-
- [1] A. E. Hosoi and L. Mahadevan, *Phys. Rev. Lett.* **93**, 137802 (2004).
- [2] J. A. Rogers, T. Someya, and Y. Huang, *Science* **327**, 1603 (2010).
- [3] O. E. Jensen, M. K. Horsburgh, D. Halpern, and D. P. Gaver, *Phys. Fluids* **14**, 443 (2002).
- [4] J. B. Grotberg and O. E. Jensen, *Annu. Rev. Fluid Mech.* **36**, 121 (2004).
- [5] D. Pihler-Puzović, P. Illien, M. Heil, and A. Juel, *Phys. Rev. Lett.* **108**, 074502 (2012).
- [6] T. T. Al-Housseiny, I. C. Christov, and H. A. Stone, *Phys. Rev. Lett.* **111**, 034502 (2013).
- [7] C. Michaut, *J. Geophys. Res.* **116**, B05205 (2011).
- [8] A. P. Bungler and A. R. Cruden, *J. Geophys. Res.* **116**, B02203 (2011).
- [9] P. G. DeGennes, *Rev. Mod. Phys.* **57**, 827 (1985).
- [10] C. Huh and L. E. Scriven, *J. Colloid Interface Sci.* **35**, 85 (1971).
- [11] D. Bonn, J. Eggers, J. Indekeu, J. Meunier, and E. Rolley, *Rev. Mod. Phys.* **81**, 739 (2009).
- [12] L. H. Tanner, *J. Phys. D* **12**, 1473 (1979).
- [13] J. C. Flitton and J. R. King, *Eur. J. Appl. Math.* **15**, 713 (2004).
- [14] See Supplemental Material at <http://link.aps.org/supplemental/10.1103/PhysRevLett.111.154501> for discussion of boundary conditions for Eq. (4), of the contact-line problem for Eq. (1), and of the experimental image processing.
- [15] A. D. McEwan and G. I. Taylor, *J. Fluid Mech.* **26**, 1 (1966).
- [16] F. Schneider, T. Fellner, J. Wilde, and U. Wallrabe, *J. Micromech. Microeng.* **18**, 065008 (2008).
- [17] Experimental parameters: with $\rho = 1.26 \text{ g cm}^{-3}$ and $B = 0.188 \text{ Pa m}^2$, the radial scale $L_e = 62.5 \text{ mm}$. For $\epsilon \equiv h_0/L_h = (0.035, 0.054, 0.151, 0.175)$, respectively, $Q = (2.493, 2.475, 2.448, 1.553) \text{ cm}^3 \text{ s}^{-1}$, $\nu = (9.52, 9.68, 9.52, 12.3) \text{ cm}^2 \text{ s}^{-1}$, and $h_0 = (260, 400, 1110, 1220) \mu\text{m}$, while the height and time scales are $L_h = (7.3, 7.4, 7.3, 7.0) \text{ mm}$ and $\tau = (11.5, 11.6, 11.6, 17.5) \text{ s}$.
- [18] For larger ϵ the early behavior of Eqs. (1) and (2) has $h \approx h_0$, and $R \propto t^{1/6}$ and $h - h_0 \propto t^{2/3}$.
- [19] L. Hocking, *Q. J. Mech. Appl. Math.* **36**, 55 (1983).
- [20] H. E. Huppert, *J. Fluid Mech.* **121**, 43 (1982).
- [21] H. M. Jensen, *Eng. Fract. Mech.* **40**, 475 (1991).
- [22] The data were scaled by $(BQ^5/\mu h_0^2)^{1/16}$ in Ref. [5].
- [23] T. T. Al-Housseiny, P. A. Tsai, and H. A. Stone, *Nat. Phys.* **8**, 747 (2012).